Mendeleev Communications

Mendeleev Commun., 2027, **37**, in press

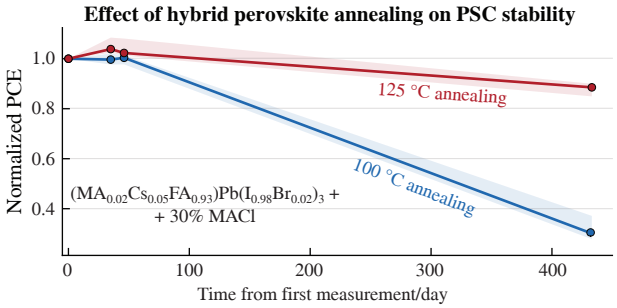
Hidden post-fabrication evolution of triple-cation perovskite solar cells controlled by annealing

Natalia N. Udalova,[a] Ekaterina I. Marchenko,[a,b] Chengyuan Wang,[a] Nikolay A. Belich,[a] Eugene A. Goodilin[a,c] and Alexey B. Tarasov*[a,c]

[a] *Department of Materials Science, M. V. Lomonosov Moscow State University, 119991 Moscow, Russian Federation. E-mail: alexey.bor.tarasov@yandex.ru*
[b] *Department of Geology, M. V. Lomonosov Moscow State University, 119991 Moscow, Russian Federation*
[c] *Department of Chemistry, M. V. Lomonosov Moscow State University, 119991 Moscow, Russian Federation*

DOI: 10.71267/mencom.8093

In perovskite solar cells (PSCs) based on triple-cation perovskite films containing 30 mol% methylammonium chloride (MACl), a hidden effect was identified, namely, the dependence of stability on annealing: insufficient thermal annealing at 100 °C leads to delayed degradation of the perovskite phase, while annealing at 125 °C for 60 min ensures the highest long-term dark storage stability of PSCs over 433 days. It was concluded that optimized annealing is not merely a crystallization step, but a key parameter determining stability and controlling hidden post-fabrication processes in MACl-assisted perovskite devices.



Keywords: perovskite solar cells, hybrid halide perovskites, stability, degradation, chloride additive.

Metal-halide perovskite solar cells (PSCs) have achieved high power conversion efficiencies;[1] however, their long-term stability is significantly influenced by the composition of the light-absorbing layer and the conditions of its formation.[2] Lead-halide perovskites with a high formamidinium (FA) content are of particular interest due to their suitable bandgap and improved thermal robustness; nevertheless, the photoactive black α-phase of $FAPbI_3$-based perovskites is metastable and requires careful stabilization.[3] To improve phase stability, performance reproducibility and device efficiency, mixed-cation perovskites with the composition $(MA_{0.02}Cs_{0.05}FA_{0.93})Pb(I_{0.98}Br_{0.02})_3$ (MA = methylammonium) have become widely adopted.[4] However, producing dense, phase-pure and morphologically uniform films from such multicomponent compositions remains a challenge due to the nature of the crystallization process and narrow processing window.

Methylammonium chloride (MACl) is one of the most common additives for controlling the crystallization of FA-rich triple-cation perovskite films.[5,6] It promotes the formation of an intermediate phase, regulates nucleation and grain growth, enhances crystallinity and facilitates the stabilization of the black perovskite phase.[5] MACl-assisted processing is successfully employed in both high-efficiency small-area devices and large-area modules, underscoring its broad technological significance.[6–8]

At the same time, the role of MACl is not limited to beneficial effects and can depend critically on the film's thermal history.[9] Since MACl is a volatile additive, annealing conditions can determine the removal of MACl-related species, local stoichiometry, residual chloride content and the formation of secondary phases.[10] Recent studies have shown that residual MA- or Cl-containing species can negatively affect operational, thermal or light stability, and that excessive or insufficient annealing can result in devices that are initially efficient but less stable.[11] Thus, MACl can act either as a powerful crystallization modifier or as a potential source of hidden degradation pathways.[12,13] Although MACl-assisted crystallization has been extensively studied, there is still no universal processing window that defines an optimal balance between MACl concentration, annealing temperature and annealing time for a given perovskite composition and device architecture.[9,14] In particular, the long-term consequences of different annealing regimes are often not apparent from initial photovoltaic parameters alone. Therefore, it is important to evaluate annealing not merely as a film formation step, but also as a factor determining film stability.

In this work, we investigated annealing as a step determining the stability of MACl-containing triple-cation lead iodide–bromide PSCs. We found that the annealing protocol dictates not only the initial device performance but also the subsequent aging pathway. By combining conventional retained-parameter analysis with time-integrated performance stability mapping developed by Udalova *et al.*,[15] this work demonstrates that the thermal history of MACl-assisted perovskite films is a critical factor governing their long-term operational potential.

The devices under study were fabricated using a perovskite with the composition $(MA_{0.02}Cs_{0.05}FA_{0.93})Pb(I_{0.98}Br_{0.02})_3$ and an excess of MACl additive (30 mol%). Perovskite films prepared from the same precursor containing excess MACl were annealed at 100 °C for 30 and 60 min or at 125 °C for 30, 45 and 60 min. All PSCs were fabricated using identical procedures with an inverted p-i-n architecture: ITO/PTAA/perovskite/C_{60}/BCP/Cu/buffer layer/cover glass, where ITO is indium tin oxide, PTAA is poly[bis(4-phenyl)(2,4,6-trimethylphenyl)amine], C_{60} is [C_{60}] fullerene, and BCP is bathocuproine. Following encapsulation,[16]

© 2027 Mendeleev Communications

the devices were stored in the dark at room temperature in accordance with the ISOS-D protocol for over 400 days.[17] Current–voltage characteristics were periodically measured for all tested PSCs using a solar simulator operating under standard AM1.5G conditions. A total of 42 encapsulated PSCs were included in the analysis of long-term dark storage data.

The initial photovoltaic parameters of PSCs, including power conversion efficiency (PCE), short-circuit current density (J_{SC}), open-circuit voltage (V_{OC}) and fill factor (FF), show a pronounced dependence on the annealing conditions of the perovskite films (Figure 1). The lowest device performance was observed for films annealed at 100 °C for 30 min, yielding an average PCE of approximately 12%. Extending the annealing time to 60 min at the same temperature resulted in a substantial improvement in PCE, driven primarily by a pronounced increase in J_{SC} [Figure 1(*b*)]. This trend suggests that a short annealing period at 100 °C is insufficient for complete perovskite conversion and/or the removal of MACl-containing intermediate phases, factors that can hinder charge transport and reduce photocurrent generation. Raising the annealing temperature further to 125 °C also strongly affected device performance; however, the effect depended on the annealing duration. Devices annealed at 125 °C for 30 min exhibited relatively high J_{SC} values but lower V_{OC} and FF values, indicating that improving photocurrent alone is insufficient to achieve high efficiency if losses due to non-radiative recombination and charge-extraction remain significant [Figure 1(*c*),(*d*)]. Extending the annealing time to 45 min and, especially, 60 min led to simultaneous improvements in J_{SC}, V_{OC} and FF, resulting in the highest PCE values, around 18%, for the 125 °C/60 min condition. These results demonstrate that the performance of MACl-assisted perovskite films is governed not only by the annealing temperature but also by the annealing kinetics, with prolonged annealing at elevated temperature promoting more complete film formation and more favorable optoelectronic properties.

Further analysis of the perovskite film's morphology and phase composition *via* scanning electron microscopy (SEM) and X-ray diffraction (XRD) revealed the presence of densely packed polycrystalline films and predominantly single-phase perovskites across all four annealing conditions (Figure 2). Within the resolution limits of these techniques, no pronounced pinholes,

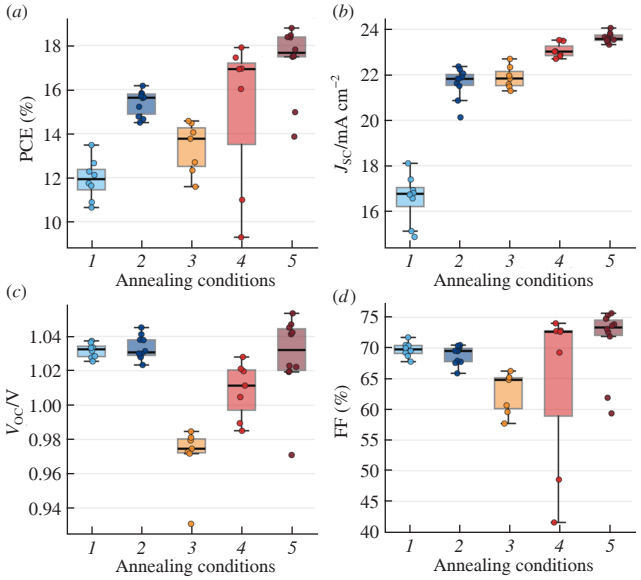


Figure 1 Statistical distribution of (*a*) PCE, (*b*) J_{SC}, (*c*) V_{OC} and (*d*) FF for PSCs fabricated under different annealing conditions (°C/min): (*1*) 100/30, (*2*) 100/60, (*3*) 125/30, (*4*) 125/45 and (*5*) 125/60.

large morphological defects or additional crystalline impurity phases were detected. Consequently, the drop in device performance observed under insufficient annealing conditions cannot be attributed to changes in surface morphology or the formation of detectable secondary crystalline phases. Instead, the performance losses are more likely related to subtler differences in the degree of film conversion, residual intermediate species, defect density and charge-transport properties, factors that cannot be directly identified through conventional SEM and XRD analysis.

An analysis of the PCE evolution of PSCs during long-term dark storage under ambient conditions revealed a pronounced dependence on the annealing conditions for the MACl-containing triple-cation perovskite films [Figure 3(*a*)]. Devices fabricated from films annealed at 125 °C retained significantly higher performance characteristics after 433 days compared to samples annealed at 100 °C. The best stability was observed for the

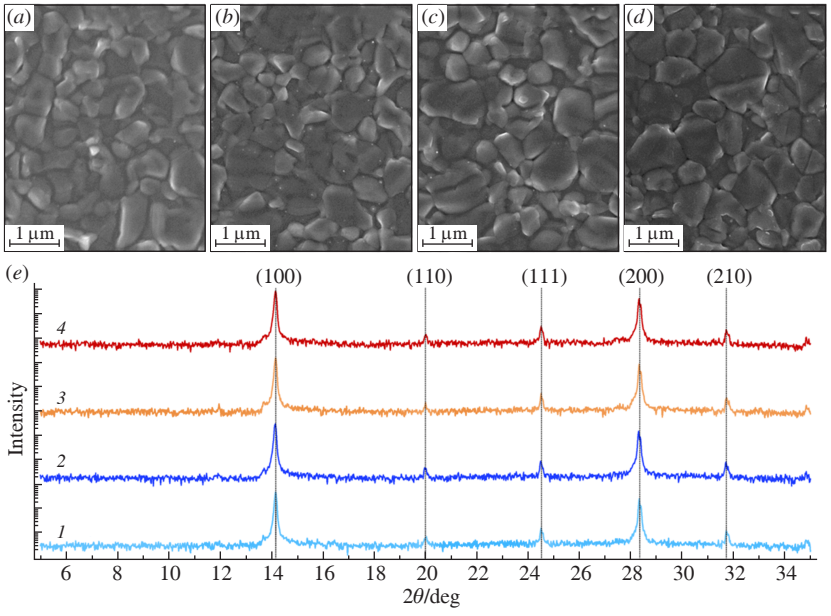


Figure 2 (*a*)–(*d*) SEM images of perovskite films with the composition $(MA_{0.02}Cs_{0.05}FA_{0.93})Pb(I_{0.98}Br_{0.02})_3$, prepared in the presence of a 30 mol% excess of MACl and annealed under the conditions (°C/min): (*a*) 100/30, (*b*) 100/60, (*c*) 125/30 and (*d*) 125/60. (*e*) XRD patterns (intensity plotted on a logarithmic scale) of the aforementioned perovskite films annealed under the conditions (°C/min): (*1*) 100/30, (*2*) 100/60, (*3*) 125/30 and (*4*) 125/60.

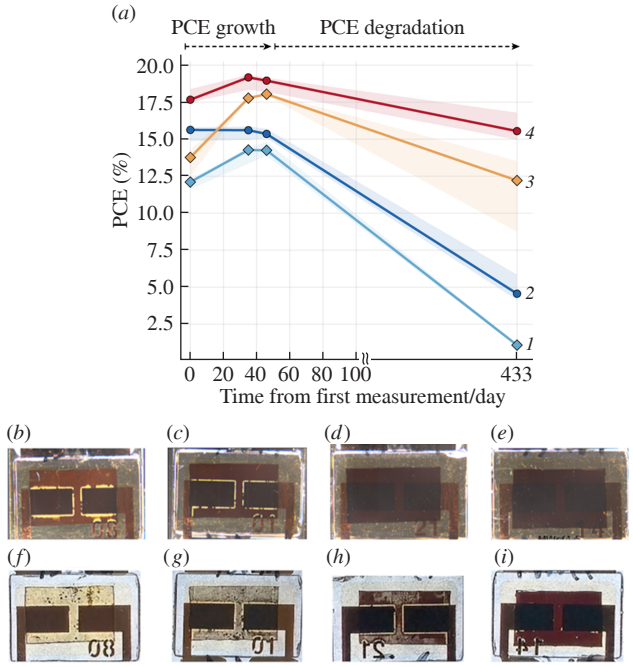


Figure 3 (*a*) Evolution of the median PCE during long-term aging according to the ISOS-D protocol for devices fabricated under different annealing conditions [°C/min (*n* per annealing group)]: (*1*) 100/30 (8), (*2*) 100/60 (10), (*3*) 125/30 (10) and (*4*) 125/60 (10). Shaded areas indicate the spread of PCE values within each group. (*b*)–(*i*) Representative photographs of devices, fabricated under different annealing conditions (°C/min): (*b*),(*f*) 100/30, (*c*),(*g*) 100/60, (*d*),(*h*) 125/30 and (*e*),(*i*) 125/60; the images were taken (*b*)–(*e*) 10 and (*f*)–(*i*) 433 days after device assembly and show visual changes in the perovskite films during long-term aging.

125 °C/60 min annealing condition: this group was characterized by high initial PCE, a moderate increase in performance during the first ~35–50 days of storage and the highest PCE level maintained by the end of the aging experiment. Devices annealed at 125 °C for 30 min exhibited similar dynamics but were prone to more pronounced long-term degradation, indicating that a shorter annealing time at this temperature is less effective for stabilizing the absorber layer. In contrast, both groups of samples annealed at 100 °C suffered severe performance losses. Although devices annealed at 100 °C for 60 min initially achieved relatively high PCE values, their efficiency dropped sharply during prolonged aging, whereas the group annealed at 100 °C for 30 min demonstrated both lower initial performance and the poorest long-term stability.

Notably, all device groups exhibit a non-monotonic, two-stage evolution of PCE. During the first ~35–50 days, the median PCE increases in almost all devices, whereas further storage leads to gradual or severe degradation, depending on the annealing conditions. This behavior indicates that slow post-fabrication processes continue within the perovskite absorber and significantly influence the long-term stability of the devices. These processes may include the redistribution or gradual removal of residual MACl-related species, ionic relaxation, defect rearrangement, partial passivation of recombination-active centers and the gradual transformation of metastable perovskite regions. The balance between these processes and irreversible degradation appears to be largely determined by annealing conditions and can dictate both the rate of the initial PCE increase and the steepness of the subsequent degradation. The extent to which these processes prove beneficial or detrimental appears to be heavily dependent on the annealing conditions. Such non-monotonic behavior should not be considered unique to this group of devices. However, most examples of non-monotonic PSC degradation reported in the literature relate to operational or light-soaking stability tests, whereas the present work focuses on the dark shelf-life aging of encapsulated, MACl-containing devices. Therefore, the observed early-stage PCE increase is interpreted as a manifestation of slow post-fabrication relaxation under dark storage conditions, rather than conventional light-induced activation.

Photographs of the devices after long-term storage further support this interpretation [Figure 3(*b*)–(*i*)]. After 433 days, devices annealed at 125 °C, particularly those annealed for 60 min, retain a darker and more uniform appearance, whereas samples treated at 100 °C exhibit pronounced visual degradation, including partial bleaching and yellowing of the perovskite layer. These changes are consistent with the degradation of the photoactive black perovskite phase and the potential formation of non-photoactive yellow δ-phase regions.[18] Thus, the initial increase in PCE during the early storage period should not be interpreted as evidence of true long-term stabilization; instead, it reflects the transient post-fabrication evolution of the perovskite film, which may be followed by substantially different degradation pathways depending on the annealing regime.

The evolution of individual photovoltaic parameters provides further insight into the non-monotonic PCE behavior observed during long-term dark storage (Figure 4). The initial increase in PCE over the first ~35–50 days is mainly accompanied by a rise in V_{OC}, whereas changes in J_{SC} and FF depend on the annealing conditions. This transient early-stage improvement may be attributed to slow post-fabrication relaxation processes, such as defect rearrangement, ion redistribution or the partial passivation of recombination-active sites, that primarily affect the open-circuit voltage.[19] Upon prolonged aging, degradation pathways become strongly dependent on annealing conditions. Devices annealed at 125 °C, especially for 60 min, retain relatively stable photovoltaic parameters, whereas the group annealed at 125 °C for 30 min suffers mainly from FF losses. In contrast, both groups of samples treated at 100 °C exhibit pronounced

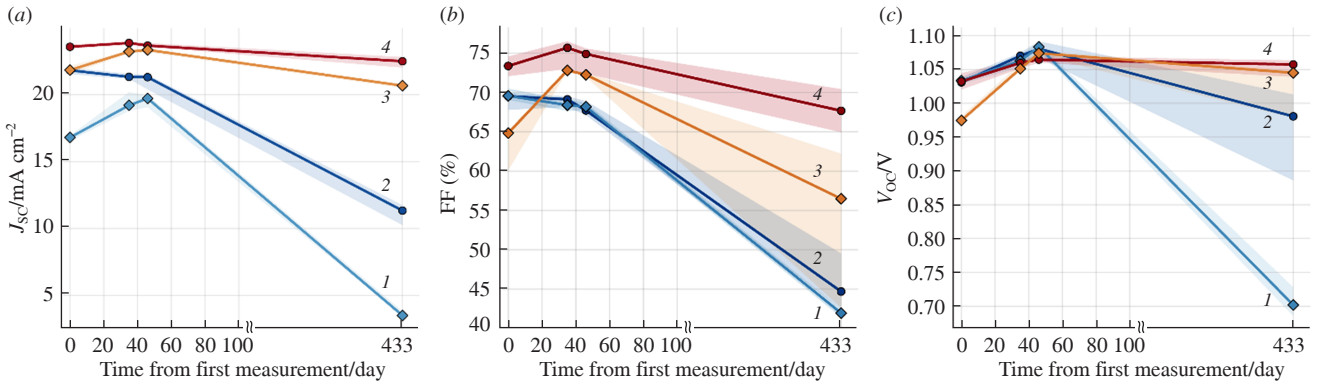


Figure 4 Time evolution of (*a*) J_{SC}, (*b*) FF and (*c*) V_{OC} for devices fabricated under different annealing conditions (°C/min): (*1*) 100/30, (*2*) 100/60, (*3*) 125/30 and (*4*) 125/60. Shaded areas indicate the spread of device parameters within each group.

degradation with significant reductions in J_{SC} and FF, consistent with the partial loss of photoactive perovskite volume observed in Figure 3(*b*)–(*i*). For samples annealed at 100 °C for 30 min, the severe loss of all *J*–*V* parameters correlates with the most pronounced transformation of the black perovskite phase into yellow, non-photoactive polymorphs. These results indicate that the early performance boost reflects transient post-fabrication relaxation rather than true long-term stabilization. Over longer aging periods, this transient improvement is followed by irreversible degradation, mainly associated with the loss of photoactive perovskite volume.

To analyze the stability behavior of devices across all groups, we employed the recently proposed TIPS(PCE) metric for time-integrated performance stability, calculated based on the PCE(*t*) trajectory.[15] This metric is defined as the integral of the PCE(*t*) curve, normalized to its maximum value, divided by the total aging time. Unlike the PCE value retained at the end of the experiment (hereinafter referred to as retPCE), which describes only the device's final state, TIPS(PCE) reflects the entire aging trajectory. Consequently, devices with similar final retained efficiencies can be distinguished if their degradation pathways during aging differ.

In this work, the stability of all tested devices was mapped using retPCE–TIPS(PCE) coordinates. As shown in Figure 5(*a*), the devices on this map are distributed along a diagonal trend line, allowing the first principal component (PC1) to serve as a stability axis. Using two empirical reference points with [retPCE, TIPS(PCE)] coordinates of (0.5, 0.5) and (0.8, 0.8), the map was divided into regions of low, intermediate and high stability. As a result, each device was assigned to one of these three regions. The resulting distribution of PSCs fabricated under different annealing conditions clearly demonstrates the impact of annealing on long-term stability: both groups of devices annealed at 100 °C fall predominantly into the low-stability region, whereas devices annealed at 125 °C occupy mainly the intermediate- and high-stability regions. Moreover, the proportion of high-stability devices increases substantially with longer annealing times at 125 °C [Figure 5(*b*)].

To illustrate that the stability map provides a meaningful classification of devices based on their degradation behavior, individual PCE degradation curves were plotted for each stability region [Figure 5(*c*)–(*e*)]. Devices categorized in the low-stability region exhibit severe performance losses during aging [Figure 5(*c*)], whereas the intermediate-stability group shows moderate degradation with partially retained performance [Figure 5(*d*)]. In contrast, devices from the high-stability region maintain substantially higher PCE values throughout the aging experiment [Figure 5(*e*)], confirming that the retPCE–TIPS(PCE) map effectively captures differences in long-term stability behavior.

Overall, the results demonstrate that annealing conditions play a key role in determining both the initial performance and long-term stability of MACl-assisted triple-cation PSCs. Although all devices were fabricated from a precursor of the same composition, their aging behavior differed strongly depending on the annealing temperature and duration. All device groups exhibited a non-monotonic evolution of PCE, characterized by an initial performance increase during the first ~35–50 days, followed by delayed degradation. This early improvement is likely attributable to slow post-fabrication relaxation processes, whereas the subsequent degradation is mainly associated with the loss of photoactive perovskite volume. Devices annealed at 125 °C, particularly those annealed for 60 min, demonstrated the most favorable stability behavior, retaining higher PCE values and more stable photovoltaic parameters after 433 days of dark storage. In contrast, insufficient annealing at 100 °C resulted in pronounced delayed degradation, despite the transient early-stage performance increase. The

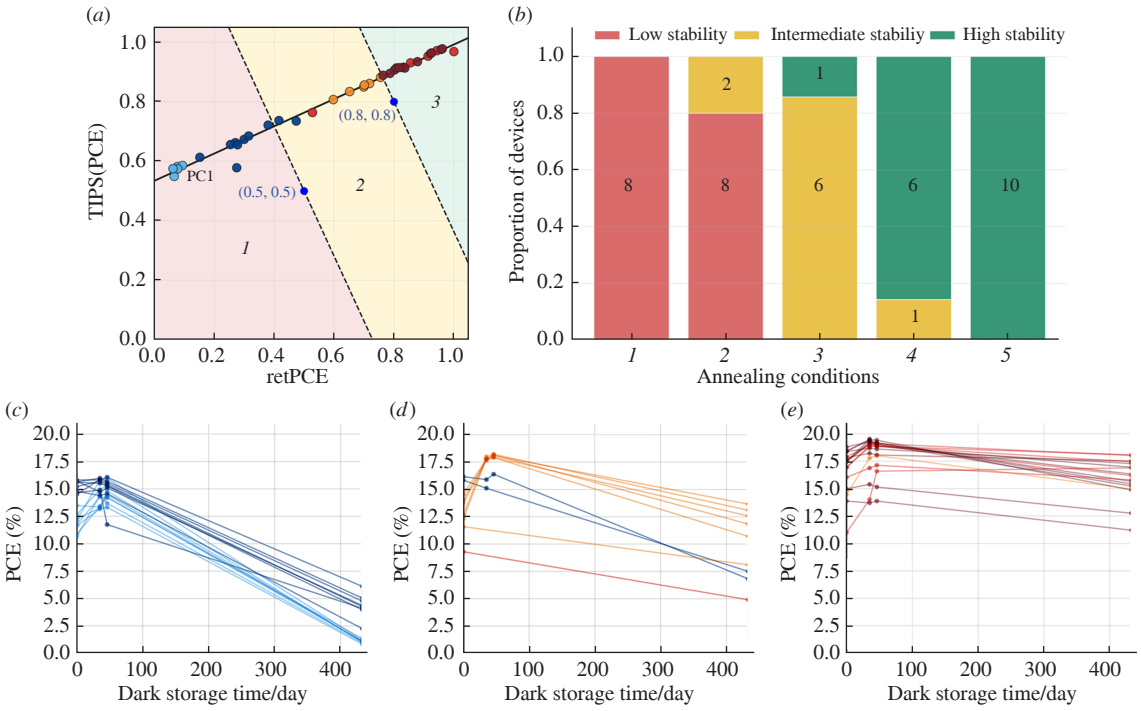


Figure 5 (*a*) Distribution of all tested devices ($n = 42$) across (*1*) low, (*2*) intermediate and (*3*) high stability regions on the retPCE–TIPS(PCE) map. The black solid line indicates the stability axis corresponding to the first principal component (PC1): TIPS(PCE) = 0.458retPCE + 0.534. Colored dots corresponds to the following annealing conditions (°C/min): 100/30 (light blue), 100/60 (dark blue), 125/30 (orange), 125/45 (red) and 125/60 (brown). (*b*) Distribution of devices fabricated under different annealing conditions [°C/min (*n* per annealing group)]: (*1*) 100/30 (8), (*2*) 100/60 (10), (*3*) 125/30 (7), (*4*) 125/45 (7) and (*5*) 125/60 (10), across low, intermediate and high stability regions. Numbers within the bars indicate the count of devices assigned to each stability region. (*c*)–(*e*) Individual PCE degradation curves for 16, 9 and 17 devices assigned to the (*c*) low, (*d*) intermediate and (*e*) high stability regions, respectively. The colored dots and lines correspond to the annealing conditions (°C/min): 100/30 (light blue), 100/60 (dark blue), 125/30 (orange), 125/45 (red) and 125/60 (brown).

retPCE–TIPS(PCE) stability mapping confirmed that this difference reflects the entire aging trajectory rather than merely the final measurement point. These findings indicate that optimizing perovskite annealing is a critical step in determining the stability of MACl-assisted PSCs.

This work was financially supported by the Russian Science Foundation (grant no. 24-73-00308). Authors acknowledge Lomonosov Moscow State University Program of Development regarding the use of the vacuum thermal evaporation unit.

Online Supplementary Materials

Supplementary data associated with this article can be found in the online version at doi: 10.71267/mencom.8093.

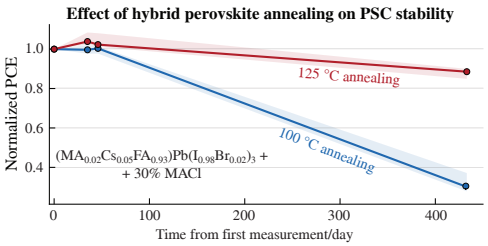
References

1 [dataset] National Laboratory of the Rockies, *Interactive Best Research-Cell Efficiency Chart*, 2026; https://www.nlr.gov/pv/interactive-cell-efficiency.
2 C. C. Boyd, R. Cheacharoen, T. Leijtens and M. D. McGehee, *Chem. Rev.*, 2019, **119**, 3418; https://doi.org/10.1021/acs.chemrev.8b00336.
3 P. E. Marchezi, E. M. Therézio, R. Szostak, H. Campos Loureiro, K. Bruening, A. Gold-Parker, M. A. Melo, Jr., C. J. Tassone, H. C. N. Tolentino, M. F. Toney and A. F. Nogueira, *J. Mater. Chem. A*, 2020, **8**, 9302; https://doi.org/10.1039/d0ta01201g.
4 M. Saliba, T. Matsui, J.-Y. Seo, K. Domanski, J.-P. Correa-Baena, M. K. Nazeeruddin, S. M. Zakeeruddin, W. Tress, A. Abate, A. Hagfeldt and M. Grätzel, *Energy Environ. Sci.*, 2016, **9**, 1989; https://doi.org/10.1039/c5ee03874j.
5 K. O. Kosmatos, L. Theofylaktos, E. Giannakaki, D. Deligiannis, M. Konstantakou and T. Stergiopoulos, *Energy Environ. Mater.*, 2019, **2**, 79; https://doi.org/10.1002/eem2.12040.
6 B. Ding, Y. Ding, J. Peng, J. Romano-deGea, L. E. K. Frederiksen, H. Kanda, O. A. Syzgantseva, M. A. Syzgantseva, J.-N. Audinot, J. Bour, S. Zhang, T. Wirtz, Z. Fei, P. Dörflinger, N. Shibayama, Y. Niu, S. Hu, S. Zhang, F. F. Tirani, Y. Liu, G.-J. Yang, K. Brooks, L. Hu, S. Kinge, V. Dyakonov, X. Zhang, S. Dai, P. J. Dyson and M. K. Nazeeruddin, *Nature*, 2024, **628**, 299; https://doi.org/10.1038/s41586-024-07228-z.
7 T. Bu, L. K. Ono, J. Li, J. Su, G. Tong, W. Zhang, Y. Liu, J. Zhang, J. Chang, S. Kazaoui, F. Huang, Y.-B. Cheng and Y. Qi, *Nat. Energy*, 2022, **7**, 528; https://doi.org/10.1038/s41560-022-01039-0.
8 N. N. Udalova, A. A. Petrov, E. M. Nemygina, K. R. Plukchi, E. A. Goodilin and A. B. Tarasov, *Mendeleev Commun.*, 2024, **34**, 840; https://doi.org/10.1016/j.mencom.2024.10.023.
9 R. Pallotta, M. Degani, F. Toniolo, S. Cavalli, F. Turci, W. H. Bi, A. Girella, C. Milanese, A. Schüler, A. Magrez and G. Grancini, *Mater. Today Adv.*, 2024, **24**, 100541; https://doi.org/10.1016/j.mtadv.2024.100541.
10 W. Song, X. Zhang, S. Lammar, W. Qiu, Y. Kuang, B. Ruttens, J. D'Haen, I. Vaesen, T. Conard, Y. Abdulraheem, T. Aernouts, Y. Zhan and J. Poortmans, *ACS Appl. Mater. Interfaces*, 2022, **14**, 27922; https://doi.org/10.1021/acsami.2c05241.
11 D.-H. Kang, S.-U. Lee and N.-G. Park, *ACS Energy Lett.*, 2023, **8**, 2122; https://doi.org/10.1021/acsenergylett.3c00568.
12 K. Zhao, L. Yao, C. Değer, X. Zhang, J. Shen, X. Miao, P. Shi, Y. Luo, D. Jin, Y. Tian, J. Xu, S. Zhang, Q. Liu, S. Chu, X. Wang, L. Tian, I. Yavuz, J. Xue and R. Wang, *Nat. Commun.*, 2025, **16**, 10074; https://doi.org/10.1038/s41467-025-65045-y.
13 B. Li, H. Wang, A. Liu, Y. Liu, W. Pu, T. Shen, M. Li, M. Que, J. Tian, Q. Dai and S. Yun, *Small*, 2023, **19**, 2301061; https://doi.org/10.1002/smll.202301061.
14 T. Maschwitz, L. Merten, F. Ünlü, M. Majewski, F. Haddadi Barzoki, Z. Wu, S. D. Öz, C. Kreusel, M. Theisen, P. Wang, M. Schiffer, G. Boccarella, G. Marioth, H. Weidner, S. Schultheis, T. Schieferstein, D. Gidaszewski, Z. Julliev, E. Kneschaurek, V. Munteanu, I. Zaluzhnyy, F. Bertram, A. Jaffrès, J. He, N. Ashurov, M. Stolterfoht, C. M. Wolff, E. Unger, S. Olthof, G. Brocks, S. Tao, H. Grüninger, O. J. J. Ronsin, J. Harting, A. F. Kotthaus, S. F. Kirsch, S. Mathur, A. Hinderhofer, F. Schreiber, T. Riedl and K. O. Brinkmann, *Nat. Commun.*, 2025, **16**, 9894; https://doi.org/10.1038/s41467-025-65484-7.
15 N. N. Udalova, E. I. Marchenko, C. Wang, N. A. Belich, E. A. Goodilin and A. B. Tarasov, *SSRN Electronic Journal*, 2026; https://doi.org/10.2139/ssrn.7520226.
16 N. A. Belich, A. A. Petrov, P. A. Ivlev, N. N. Udalova, A. A. Pustovalova, E. A. Goodilin and A. B. Tarasov, *J. Energy Chem.*, 2023, **78**, 246; https://doi.org/10.1016/j.jechem.2022.12.010.
17 M. V. Khenkin, E. A. Katz, A. Abate, G. Bardizza, J. J. Berry, C. Brabec, F. Brunetti, V. Bulović, Q. Burlingame, A. Di Carlo, R. Cheacharoen, Y.-B. Cheng, A. Colsmann, S. Cros, K. Domanski, M. Dusza, C. J. Fell, S. R. Forrest, Y. Galagan, D. Di Girolamo, M. Grätzel, A. Hagfeldt, E. von Hauff, H. Hoppe, J. Kettle, H. Köbler, M. S. Leite, S. (F.) Liu, Y.-L. Loo, J. M. Luther, C.-Q. Ma, M. Madsen, M. Manceau, M. Matheron, M. McGehee, R. Meitzner, M. K. Nazeeruddin, A. F. Nogueira, Ç. Odabaşı, A. Osherov, N.-G. Park, M. O. Reese, F. De Rossi, M. Saliba, U. S. Schubert, H. J. Snaith, S. D. Stranks, W. Tress, P. A. Troshin, V. Turkovic, S. Veenstra, I. Visoly-Fisher, A. Walsh, T. Watson, H. Xie, R. Yıldırım, S. M. Zakeeruddin, K. Zhu and M. Lira-Cantu, *Nat. Energy*, 2020, **5**, 35; https://doi.org/10.1038/s41560-019-0529-5.
18 N. N. Udalova, E. M. Nemygina, N. N. Chertorizhskiy, A. S. Tutantsev, W. Chengyuan, N. A. Belich, E. A. Goodilin and A. B. Tarasov, *J. Energy Chem.*, 2026, **117**, 355; https://doi.org/10.1016/j.jechem.2026.02.017.
19 T. Leijtens, G. E. Eperon, A. J. Barker, G. Grancini, W. Zhang, J. M. Ball, A. R. Srimath Kandada, H. J. Snaith and A. Petrozza, *Energy Environ. Sci.*, 2016, **9**, 3472; https://doi.org/10.1039/C6EE01729K.

Received: 12th May 2026; Com. 26/8093

Contents entry

Hidden post-fabrication evolution of triple-cation perovskite solar cells controlled by annealing



Natalia N. Udalova, Ekaterina I. Marchenko, Chengyuan Wang, Nikolay A. Belich, Eugene A. Goodilin, Alexey B. Tarasov